Bull. Chem. Soc. Ethiop. **2026**, 40(12), 2629-2637.
DOI: https://dx.doi.org/10.4314/bcse.v40i12.9
© 2026 Chemical Society of Ethiopia and The Authors
ISSN 1011-3924
Printed in Ethiopia
Online ISSN 1726-801X

CONVENIENT SYNTHESIS OF NEW FREE METAL DYES AND INVESTIGATION OF THE ACCEPTOR ROLE IN DYE-SENSITIZED SOLAR CELLS

Saifaldeen Muwafag Abdalhadi[1*], Asmaa Yahya Al-Baitai[2], Madeeha Hamid Mahmood[2]

[1]Department of Remote Sensing, College of Remote Sensing and Geophysics, Al-Karkh University of Science, Baghdad, Iraq
[2]Department of Chemistry, College of Science, Al-Nahrain University, Baghdad, Iraq

(Received June 7, 2026; Revised August 10, 2026; Accepted September 3, 2026)

ABSTRACT. In this study, we successfully prepared three new dyes in a one-pot reaction via the Schiff base followed by Knoevenagel reactions. The three dyes coded **SA1**, **SA2**, and **SA3** were designed with N, N-dimethylaniline as the donor, 2,2'-bipyridine as the π-bridge, and malononitrile, malonic acid, and 2-cyanoacetic acid as acceptors, respectively. Upon application to the DSSCs, the dye's properties and the solar cells' efficiencies are detailed. According to DFT modelling and electrochemical properties, **SA2** exhibits the most significant photosynthetic properties in DSSCs, which gave the highest power conversion efficiency (η = 4.47%) compared to (η = 7.91%) N719 control cell, presumably due to the tuning between the anchoring group (-COOH) and acceptor group (-CN), which promotes a better energy gap (2.54 eV), Jsc (7.36 mA.cm^{-2}), and Voc (0.88 V).

KEY WORDS: DSSCs, Acceptor, One-pot reaction, Schiff base, Knoevenagel condensation reaction

INTRODUCTION

The rising primary energy consumption caused by industrialization in developing countries, combined with the depletion of fossil fuel reserves, creates significant challenges for global energy [1-3]. Therefore, exploring renewable energy generation methods is essential. The environmental challenges associated with fossil fuel consumption and increasing CO_2 levels have led to greater attention on producing electrical energy from sustainable sources, notably solar radiation [4].

Today, silicon solar cells dominate the photovoltaic market despite their environmental impacts and high production costs [5]. Recently, Dye-sensitized Solar Cells (DSSCs) present a solution to these issues. They are cost-effective to produce, eco-friendly, and adaptable in fabrication. Unlike silicon wafer solar cells that absorb light directly, DSSCs generate electricity by converting light using photosensitive pigments and electrolyte mediators [6-9].

Metal-free dyes in DSSCs have many advantages such as lower cost, structural tunability, environmental friendliness, and simplified synthesis compared with conventional ruthenium-based sensitizers, making them attractive candidates for future DSSC technologies. Dye molecules play a vital role in light capture for DSSCs. Most reported organic dyes exhibit a donor-π-bridge-acceptor (D-π-A) structure [10], typically incorporating triarylamine-based donors due to their easy synthesis and strong electron-donating properties [11]. Cyanoacrylate derivative residues are frequently utilized as the acceptor unit because they can be easily synthesized from aldehyde residues and function as a TiO_2 anchoring unit [12-13]. Various p-conjugated bridging units, such as aromatic, heteroaromatic, and alkyne residues, have enhanced charge separation efficiency between donor and acceptor units [14-16]. In a D-π-A configuration, the acceptor units significantly influence the optical properties of the dye, prompting research to explore how various acceptor units affect the dyes' absorption characteristics and the performance of DSSCs [17-19]. Numerous researchers have demonstrated that variations in the electron-donating

*Corresponding authors. E-mail: dr.saifaldeen80@gmail.com
This work is licensed under the Creative Commons Attribution 4.0 International License

capacity of the donor component, the electron-withdrawing ability of the acceptor component, and the conjugation length of the p-bridge can result in diverse positioning of the HOMO and LUMO energy levels. This, in turn, influences the driving forces for electron injection and the modulation of the short-circuit photocurrent density (Jsc) [20-23].

This study introduces a systematic acceptor-part approach for D-π-A metal-free dyes: **SA1**, **SA2**, and **SA3**. 2,2'-bipyridine unit was selected because of its rigid conjugated structure, excellent electron-transport characteristics, and ability to enhance molecular planarity. These features facilitate intramolecular charge transfer and improve electronic communication between the donor and acceptor units. Additionally, we have examined how different acceptor groups, including malononitrile, malonic acid, and 2-cyanoacetic acid, alter the properties of the corresponding dyes and their DSSC devices.

EXPERIMENTAL

Materials and methods

All materials and solvents are supplied from Alfa Aesar® and Acros® and used without any purification. The ^{1}H-NMR and ^{13}C-NMR spectra were characterized on a Bruker Avance III 400 and recorded at 400 MHz for ^{1}H-NMR spectra and 100 MHz for ^{13}C-NMR spectra with standard TMS. The UV-vis spectra were characterized on a Perkin-Elmer Lambda 25 spectrophotometer. Mass spectrometry was performed on a Bruker MicroTOF QII. Elemental analyses (C, H, and N) were characterized using a Perkin-Elmer 240 C analyzer. The theoretical study was obtained using the Gaussian 09 software (64-bit).

Fabrication of DSSCs

DSSCs were fabricated using different dyes (**SA1**, **SA2**, and **SA3**) as an active layer. Photoanodes were prepared using TiO_2 NPs, which were made by adding absolute ethanol (3 mL) to TiO_2 powder (1.5 g, 30 to 20 nm), grinding for 5 minutes, then adding Triton X-100 (0.02 mL) and grinding for 15 minutes. The paste was subsequently coated onto a clean indium tin oxide (ITO) glass sheet (2 cm^2, 15 Ω/sq) using the doctor blade method, with a thickness of approximately 4 mm. The coated substrate was sintered on a hot plate at 80 ºC for 15 minutes, then heated to 250 ºC for 40 minutes. Once cooled, the TiO_2 layer was immersed in diluted dye solutions or N912 at each concentration (1×10^{-3} M) for about 24 hours to facilitate dye adsorption onto the TiO_2 surface. The Au counter electrode was prepared by thermal evaporation. The working electrode was then clamped with the counter electrode after adding the redox electrolyte solution (I_3^-/I^-). Finally, the assembled DSSCs were tested using photovoltaic measurement devices.

*General procedure for one-pot synthesis of compounds **SA1**, **SA2**, and **SA3***

N, N-Dimethyl-p-phenylenediamine (1.00 g, 7.34 mmol) and [2,2'-Bipyridine]-5,5'-dicarbaldehyde (1.21 g, 3.67 mmol) were dissolved in dry EtOH (50 mL) in a 2-neck flask under a nitrogen atmosphere. The mixture was stirred at 70 ºC for 3 hours. After this time, the acceptor (malononitrile, or 2-cyanoacetic acid, or malonic acid) (3.67 mmol) was added to the reaction under a nitrogen atmosphere. A few drops of piperidinium acetate were added to the mixture, then the mixture was stirred at 70 ºC for 1 hour. The mixture was cooled to room temperature, then concentrated under reduced pressure. Finally, the crude product was purified by column chromatography on silica gel (DCM : EtOAc; 3:1).

SA1 was isolated as a dark orange powder (1.09 g, 79 %), M.p 181-183 ºC,^{1}H-NMR (400 MHz, DMSO): δ 9.00 (s, 1H), 8.75 (s, 1H), 8.70 (s, 1H), 8.61 (d, J = 10.2 Hz, 1H), 8.42 (d, J = 10.2 Hz,

1H), 8.20 (d, *J* = 22.6 Hz, 1H), 8.15 (s, 1H), 7.75 (d, *J* = 22.6 Hz, 1H), 7.16 (d, *J*= 10.8 Hz, 2H), 6.66 (d, *J*= 10.8 Hz, 2H), 2.93 (s, 6H).^{13}C-NMR (100 MHz, DMSO) δ 160.58, 159.59, 155.91, 154.18, 150.67, 148.65, 147.70, 140.89, 138.30, 136.06, 132.23, 129.77, 126.95, 121.74, 115.69, 115.01, 114.62, 87.55, 41.90. HR-MS (ESI+): m/z calcd. For $C_{23}H_{18}N_6Na$ [M + Na] 401.1490 found 401.1487.

SA2 was isolated as an orange powder (1.07 g, 74%), M.p. 191-194 ºC, ^{1}H-NMR (400 MHz, DMSO) δ 9.05 (s, 1H), 8.94 (s, 1H), 8.74 (s, 1H), 8.72 (d, *J*=8.6 Hz, 1H), 8.61 (d, *J*=8.6 Hz, 1H), 8.35 (s, 1H), 8.20 – 8.16 (m, 2H), 7.15 (d, *J* = 18.1 Hz, 2H), 6.64 (d, *J* = 18.1 Hz, 2H), 2.92 (s, 6H).^{13}C-NMR (100 MHz, DMSO) δ 162.07, 160.58, 157.91, 154.18, 149.27, 148.03, 146.50, 141.81, 137.22, 136.54, 136.06, 131.23, 128.27, 127.92, 121.38, 121.01, 114.62, 111.24, 105.27, 42.88. HR-MS (ESI+): m/z calcd. For $C_{23}H_{19}N_5O_2Na$ [M + Na] 420.1436, found 420.1469.

SA3 was isolated as an orange powder (1.08 g, 71%), M.p. 198-201 ºC, ^{1}H-NMR (400 MHz, DMSO) δ 8.94 (s, 1H), 8.90 (s, 1H), 8.75 (s, 1H), 8.70 (d, *J* = 18.4 Hz, 1H), 8.62 (d, J = 18.4 Hz, 1H), 8.24 (d, *J* = 10.2 Hz, 1H), 8.19 (s, 1H), 8.01 (d, *J* = 10.2 Hz, 1H), 7.13 (d, *J* = 8.2 Hz, 1H), 6.65 (d, *J* = 8.2 Hz, 1H), 2.29 (s, 1H). ^{13}C-NMR (100 MHz, DMSO) δ 171.56, 169.28, 159.55, 156.92, 154.98, 151.77, 149.62, 146.73, 141.12, 139.31, 136.48, 132.22, 131.97, 128.72, 126.55, 122.24, 115.69, 41.81. m/z calcd. For $C_{23}H_{20}N_4O_4Na$ [M + Na], 439.1382 found 420.1390.

RESULTS AND DISCUSSION

Synthesis

Three organic dyes **SA1**, **SA2**, and **SA3** were synthesized *via* a one-pot reaction, designed using N, N-dimethylaniline as the donor, 2,2'-bipyridine as the π-bridge, and three different acceptors: malononitrile, 2-cyanoacetic acid, and malonic acid (Scheme 1). The Schiff base reaction produced the building block compound 3 with an acceptable yield, and subsequent Knoevenagel condensation with each acceptor produced dyes **SA1**, **SA2**, and **SA3** in good yields. The one-pot strategy reduces the number of purification steps, shortens reaction time, improves synthetic convenience, and provides satisfactory yields, making it an efficient route for preparing the target dyes.

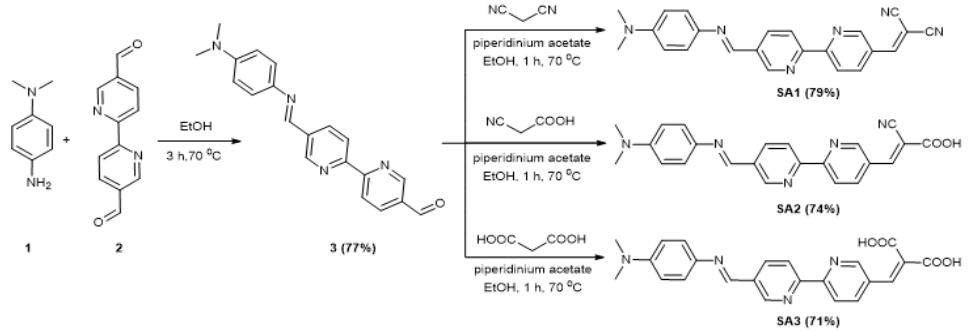

Scheme 1. Synthesis of three dyes **SA1**, **SA2**, and **SA3**.

Characterization

Figure 1 illustrates the UV-Vis absorption spectra of three dyes dissolved in dimethylformamide (DMF) as the solvent. The compounds display a pronounced absorption band within the visible spectrum, with a maximum absorption wavelength ranging from 427 to 458 nm, which is ascribed

to a π-π* transition of the conjugated aromatic moieties. The molar extinction coefficient corresponding to this wavelength demonstrates an increasing trend in the order of **SA3** < **SA1** < **SA2**. The distinctive absorption band observed in the visible region is attributed to intramolecular charge transfer (ICT) occurring between the donor and acceptor segments of the molecules. The acceptor groups affect the electron-withdrawing strength and intramolecular charge-transfer process within the D–π–A framework. The stronger electron-accepting ability of the cyanoacetic acid moiety in **SA2** enhances charge delocalization, leading to improved light absorption and a reduced energy gap compared with the other dyes. Notably, the enhanced electron-donating capacity of the Me_2N group results in a bathochromic shift of approximately 31 nm in the absorption maximum [24].

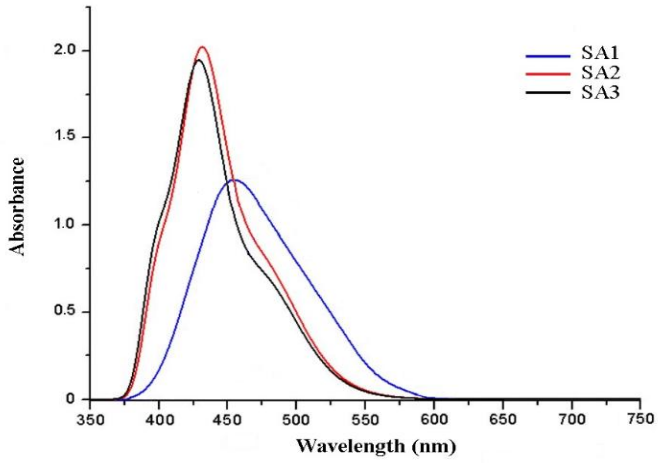

Figure 1. UV-Vis spectra of three dyes in DMF.

Theoretical study

To gain a more comprehensive understanding of the electronic properties of these dyes, computational analyses using density functional theory (DFT) and time-dependent density functional theory (TDDFT) were performed at the B3LYP/6-311G* level. Six bond lengths, labeled from L1 to L6, were used to illustrate the relationship between bond length and the dyes' donor ability. As shown in Figure 2 and Table 1, the observed gradual increase in bond lengths, especially for L3, L5, and L6 from **SA1** to **SA3**, indicates enhanced electron delocalization and intramolecular charge transfer. The elongation suggests a reduction in bond order caused by conjugation effects, which benefits light absorption and charge transport [25]. Therefore, **SA3** demonstrates the strongest conjugation and is likely to have improved photovoltaic performance. In addition, the structures of the compounds reveal that the full planarity of **SA2** and **SA3** dyes contrasts with the flipping observed in part of the acceptor group in **SA1**, directly impacting continuous conjugation from donor to acceptor. The optimized geometries indicate that **SA2** and **SA3** exhibit greater molecular planarity than **SA1**. Enhanced planarity facilitates π-electron delocalization and charge transport, contributing to improved electronic communication between donor and acceptor units and consequently better photovoltaic performance.

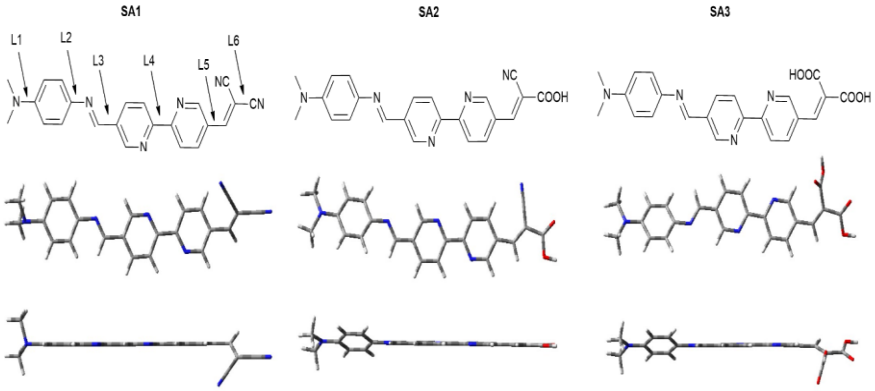

Figure 2. The optimized structure of three dyes.

Table 1. The bond lengths of three dyes, **SA1**, **SA2**, and **SA3**.

Dyes	L1(Å)	L2(Å)	L3(Å)	L4(Å)	L5(Å)	L6(Å)
SA1	1.37290	1.39948	1.44584	1.48082	1.42861	1.41984
SA2	1.37332	1.40781	1.46195	1.48137	1.44756	1.48564
SA3	1.37585	1.40964	1.46255	1.48261	1.44941	1.48953

To prepare efficient dyes in DSSCs, the Highest Occupied Molecular Orbital (HOMO) should be positioned above the conduction band of TiO_2, and the Lowest Unoccupied Molecular Orbital (LUMO) should be situated below the iodide redox potential. Figure 3 illustrates the electron distribution of HOMO and LUMO across the three dyes. For all dyes, the HOMO was delocalized within dimethylaniline and partially delocalized in bipyridine. Conversely, the LUMO was delocalized in the acceptor region and partially in the bipyridine, facilitating optimal positioning for charge and electron transfer. All LUMOs of the three dyes were positioned above the CB of TiO_2, enabling effective electron injection from the dyes to TiO_2. The energy levels were calculated theoretically for the three dyes, and the LUMO levels were similar: -3.18 eV, -3.11 eV, and -2.98 eV for **SA1**, **SA2**, and **SA3**, respectively. In contrast, the HOMO levels were shown at -5.89 eV, -5.65 eV, and -5.62 eV. The LUMO trend indicates that the malononitrile unit has the lowest electron-accepting ability among the other moieties. As shown in Table 2, energy gaps were observed, with **SA2** exhibiting the smallest value at 2.54 eV, compared to **SA1** at 2.71 eV and **SA3** at 2.64 eV. The cyanoacetic acid acceptor combines strong electron-withdrawing ability with effective conjugation and anchoring functionality, leading to enhanced intramolecular charge transfer and a reduced HOMO–LUMO energy gap

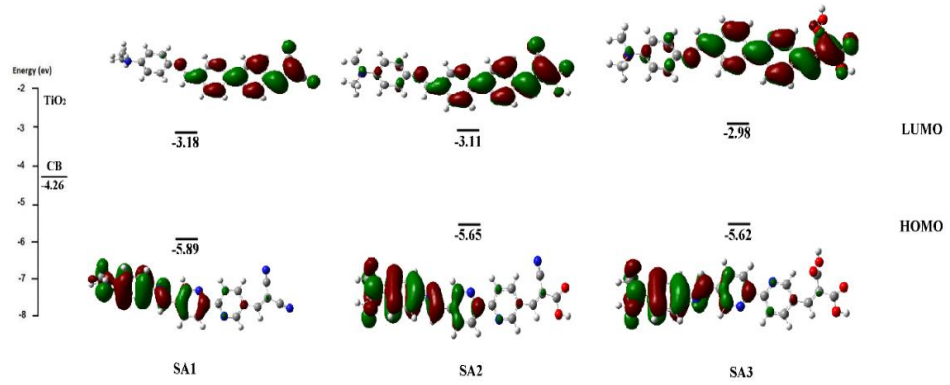

Figure 3. The electron distribution of HOMO and LUMO and their position relative to the CB of TiO_2.

Table 2. Energy gaps and NBO analysis of the three dyes in the ground state, considering q^{Donor}, $q^{\pi\text{-bridge}}$, and $q^{Acceptor}$ as the total natural charges on the donor group, π-bridge, and acceptor group, respectively.

Dye	Eg (eV)	q^{Donor}	$q^{\pi\text{-bridge}}$	$q^{Acceptor}$	$\Delta q^{D\text{-}A}$
SA1	2.71	0.0728	0.0367	-0.1097	0.1825
SA2	2.54	0.0698	0.0305	-0.1004	0.1702
SA3	2.64	0.0701	0.0283	-0.0986	0.1687

The NBO charge analysis indicates that all dyes have positive charges on the N, N-dimethylaniline part, with q^{Donor} values around +0.07 e, confirming their role as effective electron donors. The π-bridge segments also carry small positive charges, showing they act as efficient pathways for electron transfer from donor to acceptor. The acceptor groups consistently carry a negative charge, indicating electron accumulation at the acceptor ends after charge redistribution. Among the dyes, **SA1** exhibits the most negative $q^{Acceptor}$ value (−0.1097 e), implying it has the strongest electron-withdrawing capability. This stronger electron withdrawal enhances charge transfer from donor to acceptor. The charge transfer parameter Δq^{D-A}, calculated as the difference between q^{Donor} and $q^{Acceptor}$, measures intramolecular charge separation. **SA1** shows the highest Δq^{D-A} (0.1825), indicating the most efficient charge separation. Meanwhile, **SA2** and **SA3** have slightly lower but similar Δq^{D-A} values (0.1702 and 0.1687), reflecting effective but somewhat weaker charge transfer.

J–V characteristics

Table 3 summarizes the results of three dyes fabricated in DSSCs and compares them with N719 as a control. Figure (4-a) shows the J-V curve of three dyes, which was measured under one sun light AM 1.5G illumination (100 mW·cm^{-2}). All dyes showed the same photovoltaic behavior, with an initial quasi-linear photocurrent region at low bias, followed by a gradual, smooth curvature toward the open-circuit voltage (Voc), indicating efficient electron injection, stable charge generation, and the absence of current distribution.

As shown in Table 3, **SA1** exhibits the lowest power conversion efficacy (PCE) with 2.9%, and relatively lower EQE across the visible region, which could be attributed to weak anchoring attached to the surface of TiO_2, and that affects the dye absorption, which leads to a reduction in electron injection efficiency and lower Jsc (6.04 mA·cm^{-2}) and Voc (0.75 V).

In contrast, **SA2** shows the best PCE 4.47% and broadest EQE, which is attributed to the tuning between the strong acceptor of the CN group and the excellent anchoring ability of the

carboxylic acid. This characteristic enabled effective charge separation and electron injection, as well as good dye absorption, resulting in the highest Jsc (7.36 mA·cm^{-2}), Voc (0.88 V), and (FF 69 %). The enhanced Jsc value of **SA2** is mainly attributed to its broader light-harvesting capability, reduced energy gap, efficient intramolecular charge transfer, and stronger adsorption onto the TiO_2 surface through the carboxylic acid anchoring group.

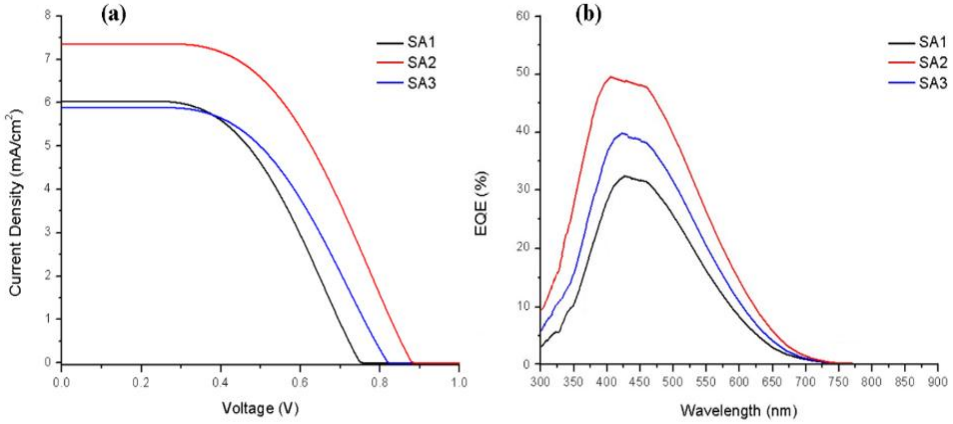

Figure 4. (a) the I-V curve of the three dyes (**SA1**: black, **SA2**: red, **SA3**: blue) under one sun illumination, (b) the IPCE spectra.

Table 3. Photovoltaic parameters of DSSCs based on different acceptor groups.

Dyes	Voc (V)	Jsc (mA·cm^{-2})	FF	PCE
N719	0.91	14.76	71%	7.91%
SA1	0.75	6.04	64%	2.90%
SA2	0.88	7.36	69%	4.47%
SA3	0.82	5.89	66%	3.19%

The **SA3** Dye with two carboxylic acids could exhibit strong chemical interaction with the TiO2 surface, with a good EQE across the visible region, which improved surface absorption and enhanced Voc (5.89 mA·cm^{-2}), Voc (0.82 V), FF (66%), resulting in a higher PCE compared to **SA1**.

Overall, the gradual increase in FF from 64% to 69% suggests improved charge transport and reduced resistive losses. The results showed that the acceptor group significantly affected the DSSC efficiencies, and the tuning between the anchoring group and the strong drawing group gave the efficiency improvement. Malononitrile exhibits strong electron-withdrawing properties; **SA1** lacks an effective anchoring group capable of strong interaction with the TiO_2 surface. Consequently, electron injection efficiency and dye adsorption are reduced, resulting in lower photovoltaic performance. The enhanced performance of **SA2** can be attributed to the synergistic combination of the cyano group, which acts as a strong electron-withdrawing unit, and the carboxylic acid group, which provides efficient anchoring onto the TiO_2 surface. This balance promotes effective charge separation, electron injection, and dye adsorption, resulting in the highest PCE among the investigated dyes. Generally, a smaller energy gap improves visible-light absorption and facilitates charge transfer processes. The reduced energy gap observed for **SA2** contributes to its superior photovoltaic performance compared with **SA1** and **SA3**.

CONCLUSION

We reported the one-pot synthesis of three D-π-A dyes featuring malononitrile, 2-cyanoacetic acid, and malonic acid as acceptor residues. The **SA2** compound with cyanoacetic acid shows high injection efficiency and the best power conversion efficiency (4.47%). The **SA1** compound shows lower conversion efficiency than **SA2** due to its poor attachment to the TiO_2 surface. Also, the **SA3** compound shows fewer electrons with the drawing group than the **SA1** dye and shows a lower power conversion efficiency than the **SA2** dye. This work suggests that the efficiency of the dyes depends on the acceptor and that this depends on the tuning between the anchoring group and the strong acceptor.

REFERENECES

1. Yakubu, S.; Samikannu, R.; Yahya, A.; Badruddin, I. A.; Kamangar, S.; Kadarmydeen, M. B.; Wetajega, S. D. Feasibility design, comparative evaluation, and energy consumption prediction of standalone hybrid energy system for rural electrification in Ghana using machine learning models. *Results Eng*. **2025**, 25, 104269-104281.
2. Bergougui, B.; Murshed, S.M.; Shahbaz, M.; Zambrano-Monserrate, M.A.; Samour, A.; Aldawsari, M.I. Towards secure energy systems: Examining asymmetric impact of energy transition, environmental technology and digitalization on Chinese city-level energy security. *Renew. Energy* **2025**, 238, 121883-121896.
3. Kartal, M.T. The role of consumption of energy, fossil sources, nuclear energy, and renewable energy on environmental degradation in top-five carbon producing countries. *Renew. Energy* **2022**, 184, 871-880.
4. Izam, N.S.M.N.; Itam, Z.; Sing, W.L.; Syamsir, A. Sustainable development perspectives of solar energy technologies with focus on solar photovoltaic: A review. *Energies* **2022**, 15, 790-803.
5. Lee, Y.J.; Kim, B.S.; Ifitiquar, S.M.; Park, C.; Yi, J.J. Silicon solar cells: Past, present and the future. *Korean Phys. Soc.* **2014**, 65, 355-361.
6. Al-Baitai, A.Y.; Mahmood, M.; Abdulhussein, S. F.; Abdalhadi, S. M. Metals doped TiO2 nanoparticle as an efficient photoelectrode in dye-sensitized solar cells: A review. *Nanochem. Res*. **2024**, 9, 207-215.
7. Abdalhadi, S.; Mohammed, N.; Ali, K.; Al-Zubaidi, H.J. Investigating the effects of fluorine substituents on organic dyes in dye-sensitized solar cells. *Turk. Chem. Soc. Sect. A Chem*. **2024**, 11, 1-10.
8. Abdulhussein, S.F.; Abdalhadi, S.M.; Hanoon, H.D. Synthesis of new imidazole derivatives dyes and application in dye sensitized solar cells supported by DFT. *Egypt. J. Chem*. **2022**, 65, 211-217.
9. Evangelista, E.; de Jesus, I.S.; Pauli, F.P.; de Souza, A.S.; Borges, A.D.A.; Gomes, M.V.S.; Forezi, L.D.S. Recent advances in the application of coumarins as photosensitizers for the construction of a dye-sensitized solar cell. *ACS Omega* **2025,** 10, 13726-13748.
10. Wu, Q.; Gao, R.; Wang, Q.; Yuan, C.; Lin, C.; Yang, Q.; Li, G. High-efficiency dye-sensitized solar cell based on carbon nanotubes-modified molybdenum nitride nanoparticles counter electrode. *Sol. Energy* **2025**, 291, 13394-13411.
11. Dalol Hanoon, H.; Muwafag Abdalhadi, S.; Hadi Ghasemi, M.; Raheem Abbas, A.; Jameel Jahil, J.; Yahya Al-Baitai, A. One-pot, efficient, and sustainable synthesis of an imidazole derivative using CuCr2O4 spinel as a catalyst. *Bull. Chem. Soc. Ethiop*. **2026**, 40, 1489-1499.
12. Fabiańczyk, A.; Gnida, P.; Chulkin, P.; Kula, S.; Filapek, M.; Szlapa-Kula, A.; Schab-Balcerzak, E. Effect of heterocycle donor in 2-cyanoacrylic acid conjugated derivatives for DSSC applications. *Sol. Energy* **2021**, 220, 1109-1119.

13. Thogiti, S.; Vuppala, S.; Cha, H.L.; Thuong, N.T.T.; Jo, H.J.; Chitumalla, R.K.; Kim, J.H.J. Photochem. Photobiol. Enhanced DSSC performance by the introduction of hydroxamic acid group into the cyanoacetic acid dyes. *A Chem.* **2020**, 398, 2512-2532
14. Ji, J.M.; Lee, H.J.; Zhou, H.; Eom, Y.K.; Kim, C.H.; Kim, H.K. Influence of the π-bridge-fused ring and acceptor unit extension in D−π–A-structured organic dyes for highly efficient dye-sensitized solar cells. *ACS Appl. Mater. Interfaces* **2022**, 14, 52745-52757.
15. Ren, Z.; Cao, Y.; Shang, C.; Sun, C. Evaluating the photoelectric performance of D-π-A dyes with different π-conjugated bridges for DSSCs. *Chem. Phys. Lett.* **2022**, 806, 140035-140051.
16. Ismaili, H.; Khalid Mustafa, S.; Jame, R.A.; Al-Aoh, H.D; Althaqafy, A.; Rehan Ajmal, M.; Islam, M. Design and multifunctional exploration of a benzophenone-based Schiff base: Synthesis, spectroscopic, DFT/TD-DFT, and molecular docking studies. *Bull. Chem. Soc. Ethiop*. **2026**, 40, 1069-1090.
17. Gong, M.; Zeng, L.; Wang, W.; Dong, X.; Yu, Z.; Wang, S.; Yang, Y. Effects of several auxiliary acceptors and anchoring groups on charge transfer and photophysical properties of D-A-π-A Type DSSCs: A DFT study. *J. Fluoresc.* **2025**, 35, 2285-2297.
18. Wang, S.; Yu, Z.; Li, L.; Qiao, J.; Gao, L. Theoretical design and analysis of D–π–A–A′ organic dyes for enhanced efficiency in DSSCs by modifying donor (D) and acceptor (A) moieties. *J. Mol. Graph. Model.* **2024**, 127, 108677-108692.
19. Abdali, S.A.; Al-Temimei, F.A.; Al-Abbas, S.S. Design a New D-π-A formation dyes as dye-sensitized solar cells applications/ a DFT and TD-DFT study. *J. Fluoresc*. **2024**, 34, 795-807.
20. Ammasi, A.; Iruthayaraj, R.; Munusamy, A.P.; Shkir, M. Molecular engineering on D-π-A organic dyes with flavone-based different acceptors for highly efficient dye-sensitized solar cells using experimental and computational study. *J. Mol. Model.* **2023**, 29, 45-64.
21. Anbarasan, P.M.; Arunkumar, A.; Shkir, M. Computational investigations on efficient metal-free organic D-π-A dyes with different spacers for powerful DSSCs applications. *Mol. Simul.* **2022**, 48, 140-149.
22. Mustafa, F.M.; Abdel Khalek, A.A.; Mahboob, A.A.; Abdel-Latif, M.K. Designing efficient metal-free dye-sensitized solar cells: A detailed computational study. *Molecules* **2023**, 28, 6177-6192.
23. Al-Fatlawe, B.A.; AL-Temimei, F.A. Design and analysis of novel D–π–A configuration dyes for dye-sensitized solar cells: A density functional theory study. *J. Comput. Electron*. **2025**, 24, 62-83.
24. Hadidi, K.; Tor, Y. Azetidines-containing fluorescent purine analogs: Synthesis and photophysical properties. *Chem. Eur. J*. **2022**, 28, 765-788.
25. Khasbaatar, A.; Xu, Z.; Lee, J.H.; Campillo-Alvarado, G.; Hwang, C.; Onusaitis, B.N.; Diao, Y. From solution to thin film: Molecular assembly of π-conjugated systems and impact on (opto)electronic properties. *Chem. Rev*. **2023**, 123, 8395-8487.